





Cite this: *Soft Matter*, 2022, 18, 2046

Received 6th December 2021,
Accepted 9th February 2022

DOI: 10.1039/d1sm01733k

rsc.li/soft-matter-journal

Non linear elasticity of foam films made of SDS/dodecanol mixtures

Raphaël Poryles, Théo Lenavetier, Emmanuel Schaub, Adrien Bussonnière,  Arnau Saint-Jalmes and Isabelle Cantat *

Foam film elasticity plays a significant role in film drainage and film stability and is thus expected to influence foam dynamical properties. It strongly depends on the foaming solution composition and differs from the interface elasticity measured in unconfined geometries. We use a deformable frame to deform an assembly of five films and we measure the tension and extension of each film. This provides a simple and accurate determination of the film elasticity, in the linear and non-linear regimes, for a set of SDS/dodecanol mixtures, at various concentrations. We show that the non-linear elastic behavior is well reproduced by Mysell's model coupled with a Langmuir coadsorption isotherm for a large range of chemical compositions.

1 Introduction

The extension of a foam film decreases the surfactant concentration at the interface, and thus increases its tension. This resistance to an area modification is the Gibbs elasticity,¹ which plays a central role in film drainage and foam stability.^{2–7} Surfactant exchanges between the bulk and the interface are very different in the presence of a large reservoir of surfactant solution, or in a thin foam film. In the second case, the total amount of surfactant in the bulk may be of the same order as the amount of surfactant at the interface, even for highly soluble surfactants. When the interface is stretched, the surfactant adsorption significantly modifies the bulk concentration and, below the critical micellar concentration, the interface concentration and the tension are modified as well. The Gibbs elasticity must therefore be measured *in situ*, in the foam film. The film tension variations induced by a film stretching have been measured in a vertical film by comparison with gravitational forces,^{8–10} or deduced from the Laplace pressure in spherical bubbles.^{7,11–13} An alternative is to measure the tension in the film of interest by comparison to the tension in neighboring films, connected to the first one along a meniscus.^{14,15} Measuring the film extension requires a well-defined closed material system to be followed during its deformation. Gravity causes internal flows in the films, and film extensions/compressions induce exchanges between the film and the menisci at its boundary, making this task challenging. Using a deformable frame supporting five connected films, coupled with a measure of the position of the menisci,

we are able to simultaneously measure the film tension and the film extension in large ranges of deformation and deformation rate.¹⁶ This is an efficient method to determine the Gibbs elasticity, and we use it in this paper to investigate the elastic properties of films made of a mixture of sodium dodecyl sulfate (SDS) and dodecanol (DOH) at various concentrations, in the linear and non-linear regimes. These solutions are classically used as foaming solutions, and dodecanol is known to modify the foam properties.¹⁷ However, the Gibbs elasticity of the foam films as a function of the dodecanol concentration was not reported in the literature. We show that the observed film elasticity can be rationalized assuming a local thermodynamical equilibrium, and a Langmuir coadsorption isotherm, if we take into account some uncertainty on the actual dodecanol concentration in the film. This modelization of the elastic behavior of a film in the non-linear regime is investigated here for the first time. Importantly, all the physico-chemical parameters used in the model have been taken in the literature and obtained from independent measures in unconfined geometries. The agreement between the model and the measures on thin films thus proves the consistency of the description of confined and unconfined systems.

2 Set-up and measurements

The set-up, shown in Fig. 1 has already been extensively described in¹⁶ and we only indicate here its main features. It consists of a deformable frame supporting five rectangular soap films connected along free menisci (also called Plateau borders). All films have a dimension $W = 60$ mm in the y direction, which is a direction of invariance of the system.

Univ Rennes, CNRS, IPR (Institut de Physique de Rennes) – UMR 6251, F – 35000 Rennes, France. E-mail: isabelle.cantat@univ-rennes1.fr

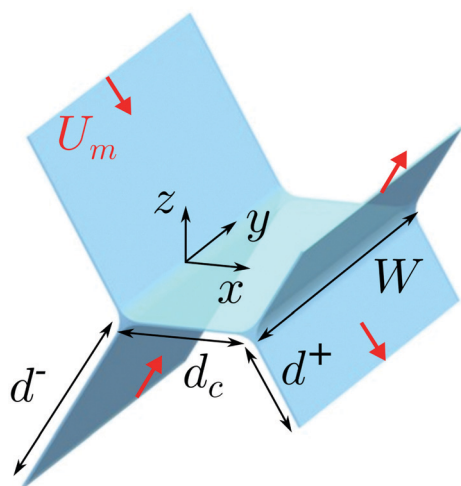


Fig. 1 Scheme of the set up and notations used in the text. The red arrows symbolised the motion of the four mobile edges.

The central film is horizontal and has a width $d_c = 6$ mm. It is connected on the left side (small x), along the left free meniscus, to the upper and lower left lateral films of width d^- and, similarly, on the right side (large x), along the right free meniscus, to the upper and lower right lateral films of width d^+ . The five films are flat and connected to each other with an angle of 120° . The width of each lateral film can be independently varied at a controlled speed using piezo-motors. As in ref. 16 the left films will be compressed while the right ones will be stretched. This symmetrical deformation conveniently keeps the central film undeformed. It thus stays at equilibrium tension and can be used as a tension reference. However, the same measure could be easily performed with only 3 films, the central one and either the compressed or the stretched lateral ones.

The foaming solutions are mixtures of Sodium Dodecyl Sulfate (SDS, BioXtra $\geq 99\%$, Sigma-Aldrich), 1-dodecanol (DOH, $\geq 98\%$, Sigma-Aldrich), glycerol (15% in volume) and fluorescein (0.8 g L^{-1}). The frame is initially plunged into a bucket containing the foaming solution. This bucket moves down at constant velocity (10 mm s^{-1}), which produces the five films. They stay at rest during 16 s and, at the reference time $t = 0$, the four motors begin to move at the velocity $U_m = 10 \text{ mm s}^{-1}$ (unless otherwise specified). The lateral film sizes varies from $d^-(0) = d_0 + A/2$ to $d^-(t^m) = d_0 - A/2$ on the left side, and from $d^+(0) = d_0 - A/2$ to $d^+(t^m) = d_0 + A/2$ on the right side. The mean size is $d_0 = 12.2$ mm and the motion amplitudes A vary in the range $[4\text{--}14]$ mm. The motors stop at the time $t^m = A/U_m$ in the range $[0.4\text{--}1.4]$ s.

Fluorescein is excited using a blue led light and is used to visualize the film thickness of the central film and the free menisci positions. The fluorescence emitted by the central film is recorded using a camera placed above the setup (MV1-D1312-160-CL12, PhotonFocus, 950×544), equipped with a green pass band filter. Another camera (ac A1920-155uc, Basler ace, 400×1920), on the left side of the device, records the vertical position of the left meniscus. Both are synchronized at

Table 1 Table of the surfactant solutions used in the paper. The first line shows the SDS concentrations rescaled by the critical micellar concentration $c_s^* = 8.1 \text{ mmol L}^{-1}$. Concentrations below and above c_s^* are separated by the double line. For two SDS concentrations, a series of mixtures has been used n at different dodecanol concentrations, given in the second line. The dodecanol molar mass is $M_d = 186.34 \text{ g mol}^{-1}$ so $c_d = 10 \text{ mg L}^{-1}$ corresponds to $c_d = 0.54 \times 10^{-4} \text{ mol L}^{-1}$. The third line provides the equilibrium surface tensions γ_0 for each SDS solutions and mixtures. They are measured with the pendant drop method 240 s after the drop formation

c_s/c_s^*	0.6	0.9	1.2	2.4	6
c_d (mg L $^{-1}$)	0	0	0-15-35	0-15-35-50	0
γ_0 (mN m $^{-1}$)	42	38	38-34-30	38-37-34-33	37

250 frames per second. The first one provides a spatial resolution of 22 pixels per mm and the other one 230 pixels per mm.

Surfactant concentrations were varied in this study and are summarized in Table 1. The concentration of SDS c_s is expressed in terms of the critical micellar concentration $c_s^* = 8.1 \text{ mmol L}^{-1}$. We used 5 different SDS concentrations in the range $[0.6\text{--}6]c_s^*$. For two series over the CMC, we added dodecanol at concentration c_d , in the range $[15\text{--}50] \text{ mg L}^{-1}$. The upper DOH concentration was imposed by the solubility limit. Under the CMC, no dodecanol was added because of its low solubility.

The initial film thickness (just before deformation) has been measured using a spectral camera (Resonon Pika L). An example of film thickness profile is shown in Fig. 2. These profiles evolve with time, because of the gravitational drainage. However, without imposed deformation, the thickness evolution is negligible during the time of the experiment (one second). The top film is always thinner than the bottom film and the average value is close to one micrometer.

2.1 Extension measurements

One difficulty of the interface extension measure is that the foam films exchange interface with the neighboring films as well as with their fixed menisci.¹⁸ When the left film is compressed, the tension becomes lower in the left film than in the central film (for non-negligible film elasticity), and the top interface slides across the left meniscus, from the top left

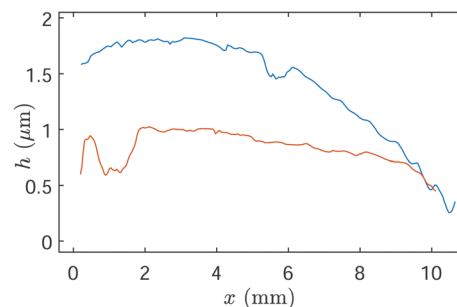


Fig. 2 Film thickness profiles before deformation for the top (red) and bottom (blue) films, for the case $c_s = 2.4c_s^*$ and $c_d = 50 \text{ mg L}^{-1}$. The average thicknesses are respectively $0.8 \mu\text{m}$ and $1.2 \mu\text{m}$ for the top and bottom films.

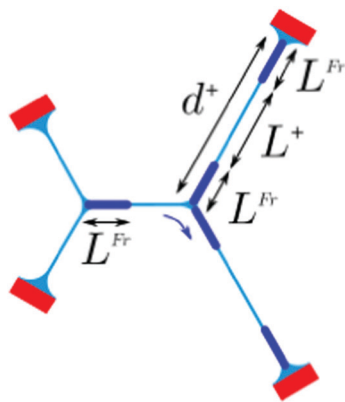


Fig. 3 Sketch of the films, after the deformation (not to scale). The light blue lines are the films initially present, less than one micron thick, and the dark blue lines represent the films extracted from the menisci, the Frankel's films, a few microns thick. The free menisci at the intersection of three films, and the meniscus on the solid frame (in red) have a diameter of 300 μm . At the free menisci, the film extraction is coupled to an interface transfer from the left films to the central one, and from the central film to the right ones, symbolized by the dark blue arrow.

film to the central film. Symmetrically, the bottom interface slides from the bottom left film into the central film. When exiting the meniscus, these interfaces drag some solution, leading to the apparition of a micron-thick piece of film in the central film, called the Frankel's film,¹⁹ as schematized in Fig. 3. Its size in the x direction is denoted as L^{Fr} in the following. It corresponds to the interface area lost by the left films by transfer to the central film. The same transfer process occurs at the right meniscus, between the central film and the right films. The overtension in the right films also induces a Frankel's films extraction from the top right and bottom right menisci, as shown in Fig. 3, corresponding to some interface directly provided by these supported menisci. We show in ref. 18 that, at short times, all these interface transfers have the same amplitude, as shown in Fig. 3, and correspond to the area lost or gained by each film. As a consequence, the film extension can be measured as

$$\begin{aligned}\varepsilon^- &= \frac{d^- + 2L^{\text{Fr}}}{d^-(0)} - 1 \\ \varepsilon^c &= \frac{d^c - L^{\text{Fr}} + L^{\text{Fr}}}{d^c(0)} - 1 = 0 \\ \varepsilon^+ &= \frac{d^+ - 2L^{\text{Fr}}}{d^+(0)} - 1\end{aligned}\quad (1)$$

The distances $d^\pm(t)$ are controlled by the motor motion and the width $L^{\text{Fr}}(t)$ is measured from the fluorescence images of the central film. The definitions given by eqn (1) are only valid if the Frankel's film remains invariant by translation in the y direction, which is carefully checked on the image, and if $L^{\text{Fr}}(t)$ is small enough (see ref. 18). The measure is therefore stopped

when $L^{\text{Fr}}(t)$ reaches a maximal value (close to 1 mm for each series).

2.2 Tension measurements

We define the film tension as the force per unit length resulting from the contributions of both interfacial tensions and of the pressure P in the film (see Fig. 4). In the imposed deformation regime, the air pressure is uniform and its value is used as reference pressure, so $P = 0$ in the gas phase. The airborne viscous forces are negligible as well as the film inertia and weight, so the only force acting on the film is its tension, which is thus uniform in each individual film.^{14,16} As measured in,¹⁸ the central film is not deformed, so its tension is the equilibrium film tension σ_0 . The film tensions, denoted as σ^- and σ^+ respectively in the compressed and stretched films, are deduced from the angle θ^- and θ^+ defined in Fig. 4

$$2\sigma^\pm \cos\theta^\pm = \sigma_0. \quad (2)$$

The vertical displacement of the meniscus is less than 10% of the horizontal one, which shows that the top and bottom film tensions are very close, with a difference smaller than our error bar, so we do not distinguish between both values. Moreover, the film curvatures are checked to be negligible, so the two out-of-equilibrium angles only depend on the meniscus displacement δ^- and δ^+ measured with the top camera

$$\theta^\pm = \tan^{-1}\left(\frac{d^\pm \sin\theta_0}{d^\pm \cos\theta_0 + \delta^\pm}\right). \quad (3)$$

The measure of the out of equilibrium angles leads to a measure of the relative film tension variation $\Delta\sigma/\sigma_0$, with $\Delta\sigma$ defined as $\sigma^+ - \sigma_0$ or $\sigma^- - \sigma_0$, respectively for the extension and compression cases:

$$\frac{\Delta\sigma^\pm}{\sigma_0} = \frac{1}{2\cos\theta^\pm} - 1. \quad (4)$$

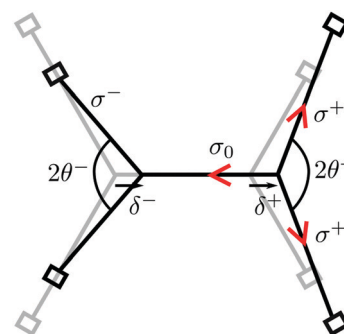


Fig. 4 Sketch of the film assembly, before (gray) and after (black) deformation. The angles θ^+ and θ^- are deduced from the meniscus displacement δ^- and δ^+ . The film tensions σ^- and σ^+ are deduced from the force balance on the each meniscus (symbolized, for the right meniscus, by the three red arrows).

3 Film tension and elasticity

The elastic behavior of the films is given by the relationship between the film tension given by eqn (4) and the film deformation given by eqn (1). An example is shown in Fig. 5. The positive tensions are measured on the right films and the negative ones are measured on the left films. The two graphs in Fig. 5(a) have been obtained with a motor velocity of 5 and 10 mm s⁻¹, and are superimposed. This confirms that the film extension rate has a negligible influence on the film tension as established in.¹⁶ A non-linear elastic regime is reached at high deformation: the tension increases sublinearly in extension and superlinearly in compression.

The film tension σ is simply given by $\sigma = 2\gamma$, with γ the interfacial tension. It can be easily expressed as a function of the film extension for a single species, in the absence of exchange with the bulk, and for a linear constitutive law $\Delta\gamma = -E^{\text{lin}}\Delta\Gamma/\Gamma_0$ between the surface tension and the excess

concentration Γ , with Δ indicating a variation with respect to an equilibrium situation. In that case,^{9,16,20}

$$\frac{\Delta\sigma}{\sigma_0} = \frac{E^f}{\sigma_0} \frac{\varepsilon}{1 + \varepsilon}, \quad (5)$$

with $E^f = 2E^{\text{lin}}$ the film elasticity.

In this relation, the mass conservation on a piece of film of initial interface area A_0 imposes $\Gamma_0 A_0 = \Gamma A = \Gamma A_0(1 + \varepsilon)$, and thus $\Delta\Gamma/\Gamma_0 = -\varepsilon/(1 + \varepsilon)$. The initial linear law coupling the tension and the surface excess is transformed into the non linear eqn (5) due to this single effect.

Before addressing in Section 4.1 the whole non linear thermodynamical model, we first extract a phenomenological film elasticity E^f by fitting our data by the eqn (5), for all foaming solutions of Table 1. The experimental data and the fitting curves are plotted in Fig. 5(b), for one series, showing that the non-linearity is captured by eqn (5), as already observed in.¹⁶

The obtained film elasticity E^f , normalized by the equilibrium film tension, is plotted in Fig. 6(a) as a function of the SDS concentration, for the series without added dodecanol. Below the CMC, the elasticity decreases with the SDS

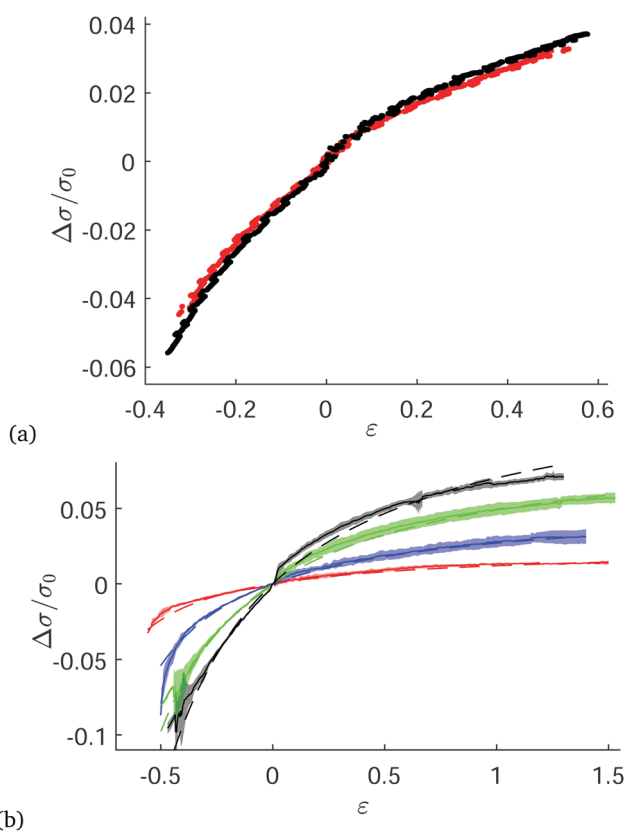


Fig. 5 Relative film tension variation as a function of the film extension. The compressed and stretched films correspond respectively to negative and positive values. (a) The concentrations are $c_s = 2.4c_s^*$ and $c_d = 35 \text{ mg L}^{-1}$. The amplitude of the motor motion is $A = 6 \text{ mm}$ and the motor velocity is $U_m = 5 \text{ mm s}^{-1}$ (●) and 10 mm s^{-1} (●). The error bar is below 5% for each quantity. (b) The concentrations are $c_s = 2.4c_s^*$ and $c_d = 0 \text{ mg L}^{-1}$ (red), $c_d = 15 \text{ mg L}^{-1}$ (blue), $c_d = 35 \text{ mg L}^{-1}$ (green), $c_d = 50 \text{ mg L}^{-1}$ (black). The solid lines represent the average values and the shaded areas are the standard deviations. The dashed lines are the relation 5, with $E^f/\sigma_0 = 0.024, 0.054, 0.098, 0.14$.

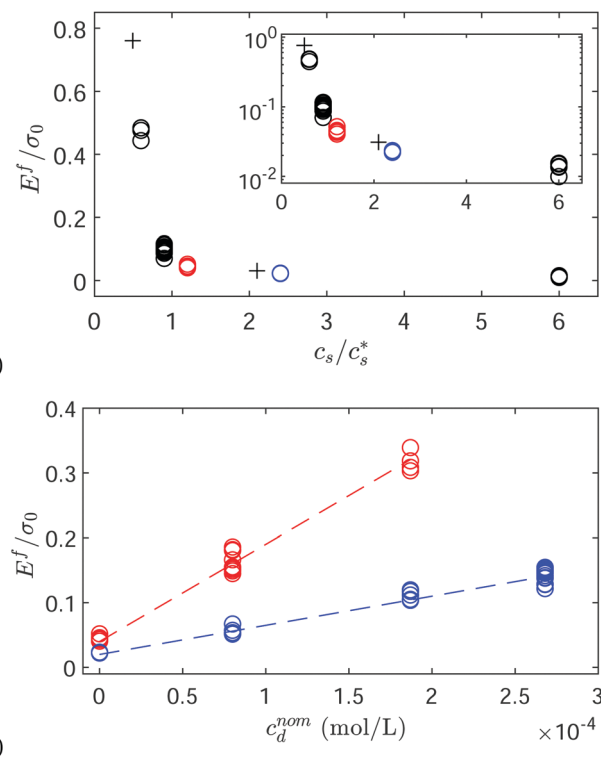


Fig. 6 Film elasticity E^f rescaled by the equilibrium film tension $\sigma_0 = 2\gamma_0$. (a) E^f/σ_0 as a function of the SDS concentration, for a DOH nominal concentration equal to zero. The circles are our original data points obtained at various amplitudes of deformation. The red and blue circles are the same as the points at $c_d^{\text{nom}} = 0$ in the graph (b). The + are data from ref. 9 (Table 1, $h = 1.13 \mu\text{m}$). The inset shows the same data in a semilog representation. (b) E^f/σ_0 as a function of the nominal dodecanol concentration for the SDS concentrations $c_s = 1.2c_s^*$ (in red) and $c_s = 2.4c_s^*$ (in blue). The dashed lines are fitted affine laws.

concentration. Note that for a single interface, the elasticity first increases with the concentration at low concentration and then decreases when approaching the CMC.^{21,22} However, at very low concentration the films are not stable anymore and only the decreasing part of the curve is observable here. Above the CMC, the elasticity becomes much smaller than σ_0 , but is still measurable, which is unexpected for a solution of pure SDS above the CMC. Indeed, already for the case $c_s = 1.2c_s^*$, the bulk concentration is high enough to remain above the CMC despite the surfactant adsorption at the interface, at least below a critical extension. The interface should thus remain saturated at a constant concentration, and stay at tension $\gamma(c_s^*)$ whatever ε , leading to $E^f = 0$. This is not compatible with the measurements. We attribute this result to the presence of traces of insoluble species, potentially DOH mixed with the SDS. In the following, we will distinguish between the nominal DOH concentration given in Table 1 and the actual, unknown, DOH concentration. As shown in Fig. 6(a), the obtained elasticity values are in good agreement with the ones reported in,⁹ for the same solution and the same thickness range.

In Fig. 6(b), we show the film elasticity as a function of the nominal DOH concentration for the two SDS concentrations larger than the CMC. A linear increase is measured for both series, with a slope decreasing with the SDS concentration. This can be explained by the fact that most of the dodecanol is solubilized in the SDS micelles. The free dodecanol monomers are in equilibrium with the dodecanol in the micelles and are less numerous, for a given dodecanol concentration, when a larger number of micelles is available. At constant dodecanol bulk concentration, the dodecanol surface excess thus decreases with the SDS concentration above the CMC, and its contribution to the elasticity decreases as well.

The aim of the next section is to provide a more quantitative analysis of these observations and to predict the measured elasticities on the basis of the thermodynamics laws governing surfactant mixtures.

4 Non-linear film elasticity prediction

4.1 Thermodynamical model

The interfacial properties of SDS/dodecanol mixtures have been intensively investigated, because of their practical interest. The Frumkin model allows us to reproduce quantitatively the curves of the tension as a function of the bulk concentration.²³ However, the theoretical modeling of the coadsorption is difficult to address using this model and a simplified approach, relying on a Langmuir coadsorption isotherm, is used in the literature. In that frame, a reduced number of parameters can be defined to rationalize the data obtained in a large range of concentrations for both species. The model used in²³ is presented below and used to rationalize our experimental data.

4.1.1 Adsorption laws. The surface active components in the solutions are the dodecanol of bulk concentration c_d and surface excess Γ_d , and the SDS of bulk concentration c_s and

surface excess Γ_s . The SDS has a critical micellar concentration c_s^* and its monomeric concentration c_s^m verifies

$$c_s^m = c_s \quad \text{if} \quad c_s < c_s^* \quad \text{and} \quad c_s^m = c_s^* \quad \text{otherwise.} \quad (6)$$

The amount of SDS in the micellar form is denoted c_s^M , so $c_s^M + c_s^m = c_s$. When $c_s^M > 0$, a part of the dodecanol is embedded in the SDS micelles.²⁴ A simple law of mass action is assumed to govern the equilibrium between the monomeric concentration c_d^m and the concentration in the micelles c_d^M so $c_d^M = Kc_d^m c_s^M$ and, using $c_d^M + c_d^m = c_d$, we get

$$c_d = c_d^m(1 + Kc_s^M). \quad (7)$$

Finally, the SDS is an anionic surfactant, assumed to be entirely dissociated. Its counterion Na^+ does not have any interfacial property, but the electroneutrality imposes that its concentration around the micelles c_n^M , its concentration dispersed in the bulk c_n^m and its interfacial excess Γ_n verify $c_n^M = c_n^m$, $c_n^m = c_n^m$ and $\Gamma_n = \Gamma_s$.

The equilibrium between the monomers in solution and the interface is assumed to be governed by Langmuir isotherms. For each species of index $i = \{s, d, n\}$ the adsorption and desorption fluxes j_i^+ and j_i^- are

$$j_i^+ = k_i^+ c_i^m \left(\Gamma_\infty - \sum_k \Gamma_k \right), \quad (8)$$

$$j_i^- = k_i^- \Gamma_i \quad (9)$$

The equilibrium surface excesses, solutions of the equations $j_i^+ = j_i^-$, are

$$\Gamma_d = \Gamma_\infty \frac{K_d c_d^m}{1 + 2K_s c_s^m + K_d c_d^m}, \quad (10)$$

$$\Gamma_s = \Gamma_\infty \frac{K_s c_s^m}{1 + 2K_s c_s^m + K_d c_d^m}, \quad (11)$$

where we define the affinities $K_i = k_i^+/k_i^-$.

4.1.2 Mass conservation. We verified in¹⁶ that the film deformations are perfectly reversible and that the film tension does not depend on the film extension rate but only on the extension. This confirms the assumptions made in^{9,20} that the characteristic times of diffusion along and across the film are respectively much larger and much smaller than the time scale of the imposed deformation, and thus associated with a negligible dissipation. This also implies that intrinsic interfacial and bulk viscosities are negligible.

Under these assumptions each film element, spanning from one interface to the other, of thickness h and of volume $d\Omega = hdS$, is a closed system, with the interfaces at chemical equilibrium with the underlying bulk. The bulk concentrations and surface excesses can thus be deduced from the mass conservation of each species:

$$2(\varepsilon+1)\Gamma_d + c_d h_0 = 2\Gamma_{d,0} + c_{d,0} h_0, \quad (12)$$

$$2(\varepsilon+1)\Gamma_s + c_s h_0 = 2\Gamma_{s,0} + c_{s,0} h_0, \quad (13)$$

with the subscript 0 indicating the reference value before deformation, and with the deformation ε defined as $\varepsilon = (dS - dS_0)/dS_0$.

4.1.3 Gibbs law. In order to determine the interfacial tension as a function of the film deformation, the monomeric concentrations are first determined numerically as a function of the deformation and of the initial bulk concentration $c_{s,0}$ and $c_{d,0}$ in the film, using the closed equation set (6), (7), (10)–(13).

The surface tension γ is then obtained from the Gibbs adsorption law

$$d\gamma = - \sum_i \Gamma_i d\mu_i = - \sum_i \Gamma_i d(\ln c_i^m). \quad (14)$$

which can be integrated, using eqn (10) and (11) in the form

$$\gamma = \gamma_w - RT\Gamma_\infty \ln(1 + 2K_s c_s^m + K_d c_d^m), \quad (15)$$

with γ_w the surface tension of pure water.

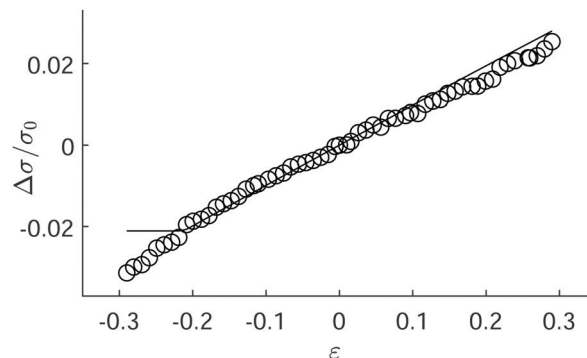
4.2 Comparison with the experimental data

4.2.1 Parameters of the model. The model depends on four parameters, Γ_∞ , K_d , K_s and K , which we took from the literature. They can be deduced from the measurement of the surface tension^{9,23–27} or of the surface excess²⁸ at the surface of bulk liquid. The reported parameters show some variability from one experiment to the other (see the review of the parameters found in the literature in Table 2), and a more refined model would probably be necessary to reconcile all data. In particular, we could consider a Frumkin adsorption model, and/or the presence of a SDS/dodecanol complex in the bulk, as assumed in.²⁸

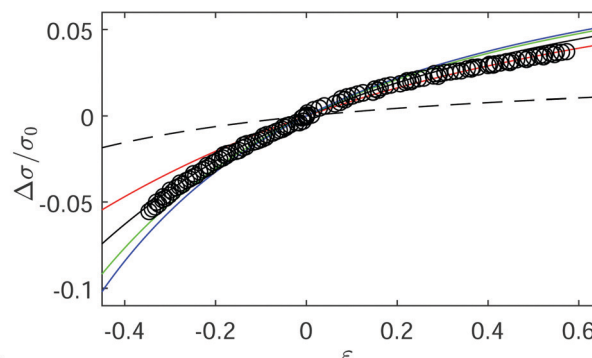
To fit our data, we took $c_s^* = 8.1 \text{ mol m}^{-3}$, $\Gamma_\infty = 6.5 \times 10^{-6} \text{ mol m}^{-2}$, $K_s = 0.14 \text{ m}^3 \text{ mol}^{-1}$, $K_d = 98 \text{ m}^3 \text{ mol}^{-1}$ as measured in²³ and $K = 4.67 \text{ m}^3 \text{ mol}^{-1}$ as measured in.²⁴

The top and bottom film thicknesses are not identical (see Fig. 2). However, we verify in Fig. 7 that their difference leads to a negligible variation of the film elasticity, which is consistent with the small value of the vertical meniscus motion discussed in Section 2.2. In the model, we use $h = 1 \text{ }\mu\text{m}$, which is close to the average film thickness for all solutions.

Finally, as already noted in Section 3, the model is incompatible with the non-zero elasticity measured for a SDS concentration above the CMC and without added dodecanol. Consequently, we propose to interpret our data either using the nominal dodecanol concentrations c_d^{nom} or using an



(a)



(b)

Fig. 7 Relative film tension variation as a function of the film extension. (a) $c_s = 0.9c_s^*$, $c_d^{\text{nom}} = 0 \text{ mg L}^{-1}$. The solid line is the prediction of the model with $c_d^{\text{fit}} = c_d^{\text{nom}} = 0 \text{ mg L}^{-1}$. (b) $c_s = 2.4c_s^*$, $c_d^{\text{nom}} = 35 \text{ mg L}^{-1}$. The solid lines are the prediction of the model with $c_d^{\text{fit}} = 153 \text{ mg L}^{-1}$ and $h = [0.3-0.5-1-2] \text{ }\mu\text{m}$, respectively for the blue, green, black and red lines. The dashed line is the prediction of the model using $c_d^{\text{nom}} = 35 \text{ mg L}^{-1}$.

adjustable dodecanol concentration c_d^{fit} , fitted on the experimental data.

4.2.2 Predictions of the model. The system is solved with a Matlab code using the parameters given in section 4.2.1. The tension obtained numerically is plotted as a function of the film extension in Fig. 7 and compared with the experimental results for two sets of concentrations, above and below the CMC.

For the case $c_s = 0.9c_s^*$ and $c_d^{\text{nom}} = 0$, the prediction of the model is quantitative, as shown in Fig. 7(a). However, the agreement is less good for the other concentration sets, as seen in Fig. 7(b). In this case, the experimental tension is larger than the predicted one, and a quantitative agreement is only

Table 2 Table of the co-adsorption Langmuir parameters found in the literature, by chronological order. Most parameters are deduced by the authors from comparison with their experimental data, but some are taken from the previous articles ('from lit.') and some are not given in the paper but can be deduced from the data ('from data'). The values used in²⁸ are not reported as a SDS/dodecanol complex is assumed, preventing a direct comparison

	Γ_∞ (mol m ⁻²)	K_s (m ³ mol ⁻¹)	K_d (m ³ mol ⁻¹)	K (m ³ mol ⁻¹)	c_s^* (mol m ⁻³)
van den Tempel <i>et al.</i> ²⁵	2.5–5 × 10 ⁻⁶	5			
Prins <i>et al.</i> ⁹	7 × 10 ⁻⁶	0.38	233		5
Joos <i>et al.</i> ²⁶	7 × 10 ⁻⁶ (from lit.)				8
Vollhardt <i>et al.</i> ²⁷	14 × 10 ⁻⁶ (from data)	0.13	98		8.1
Fang <i>et al.</i> ²⁴	6 × 10 ⁻⁶ (from lit.)	0.78 ou 0.48	1600	4.67 or 5.83	5 or 8.1
Vollhardt <i>et al.</i> ²³	6.5 × 10 ⁻⁶	0.13 (from lit.)	98 (from lit.)		7–8

obtained using a dodecanol concentration c_d^{fit} larger than the nominal one.

The overall nonlinearities are well captured by the model for all concentration sets, when an adjustable dodecanol concentration is used. Note that, for $c_s = 0.9c_s^*$, the bulk SDS concentration is close enough to the CMC so that $c_s = c_s^*$ is numerically reached in the bulk when $\varepsilon = -0.2$. Indeed the film compression leads to SDS desorption and to a bulk concentration increase in the film. At this critical point, the model predicts that the film tension should saturate at its CMC value, which explains the kink in the theoretical graph in Fig. 7(a). This predicted singular behavior is not observed experimentally.

At small deformation, the linear elastic behavior of the film can be described by the law $\sigma = E^{\text{f,th}}\varepsilon$, with $E^{\text{f,th}}$ the theoretical elastic modulus of the film, obtained from a linear fit of the numerical result. We first discuss the results obtained using the nominal dodecanol concentration, *i.e.* without adjustable parameter. The theoretical elasticity values are shown in Fig. 8 as a function of the nominal dodecanol concentration and can be directly compared with the experimental values shown in Fig. 6(b). The variation of the modulus is qualitatively reproduced: the modulus increases almost linearly with the dodecanol concentration and decreases with the SDS concentration. However, the elasticities are underestimated, especially for $c_s = 2.4c_s^*$.

Below the CMC, the model predicts that the rescaled film elasticity increases with the SDS concentration and suddenly falls to zero at the CMC. A fast decrease is indeed observed close to the CMC in Fig. 6(a), but the theory does not reproduce the elasticity decreases observed between $c_s = 0.6c_s^*$ and $c_s = 0.9c_s^*$.

Finally, the model reproduces some key features, especially the dominant role of the dodecanol above the CMC, and the linear dependency of the elasticity with the dodecanol concentration. However, a quantitative agreement with all the experimental data can only be obtained if the dodecanol concentration is fitted.

In Fig. 9 we plot the fitted dodecanol concentration for all the foaming solutions. The dashed line corresponds to

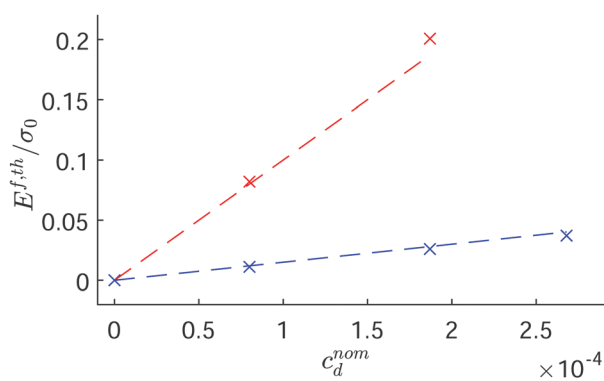


Fig. 8 Theoretical film elasticity, rescaled by the film tension, as a function of the dodecanol concentration for $c_s = 1.2c_s^*$ (in red) and for $c_s = 2.4c_s^*$ (in blue). The dashed lines are linear fits.

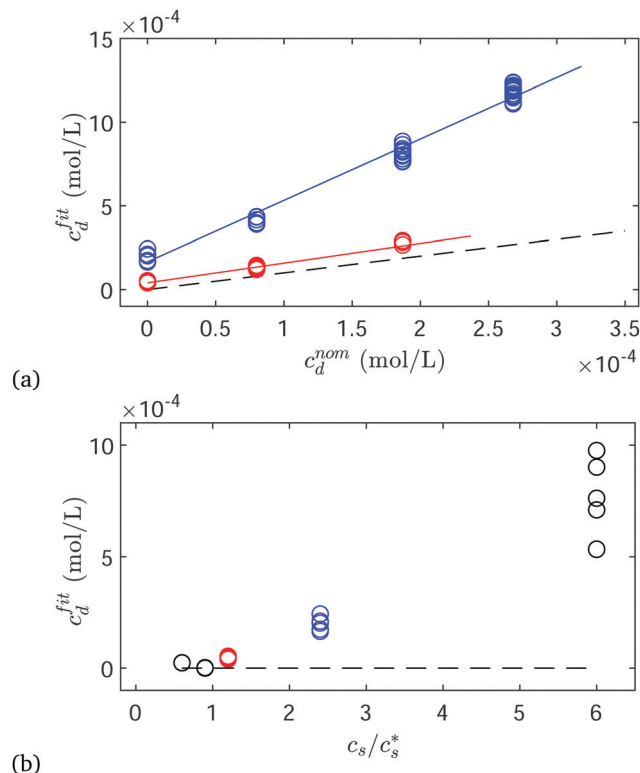


Fig. 9 Fitted dodecanol concentration obtained for the different solutions. In both graphs, the dashed line corresponds to $c_d^{\text{fit}} = c_d^{\text{nom}}$. (a) c_d^{fit} as a function of the nominal dodecanol concentration for the SDS concentrations $c_s = 1.2c_s^*$ (in red) and $c_s = 2.4c_s^*$ (in blue). (b) c_d^{fit} as a function of the SDS concentration, for a DOH nominal concentration equal to zero. The red and blue points in the graph (b) are the same as the points at $c_d^{\text{nom}} = 0$ in the graph (a).

$c_d^{\text{nom}} = c_d^{\text{fit}}$ and all the fitted values are above the nominal one. The series below c_s^* and at $1.2c_s^*$ are very close to the dashed line, which is the expected value. The best affine fit for the data at $c_s = 1.2c_s^*$ is $c_d^{\text{fit}} = 1.2c_d^{\text{nom}} + c^{\text{res}}$, with $c^{\text{res}} = 4 \times 10^{-5} \text{ mol L}^{-1}$.

For larger SDS concentrations the fitted dodecanol concentration is significantly larger than the nominal concentration. In particular, the slope of the affine fit $c_d^{\text{fit}} = 3.6c_d^{\text{nom}} + c^{\text{res}}$, with $c^{\text{res}} = 0.2 \times 10^{-3} \text{ mol L}^{-1}$, obtained for $c_s = 2.4c_s^*$, cannot be explained by a residual dodecanol concentration in the SDS only. This may indicate that the value of the dodecanol solubility in the micelles K is overestimated. Indeed, for SDS concentrations above the CMC, if K increases, the dodecanol free monomer concentration decreases (for a given total dodecanol concentration). The theoretical elasticity is thus a decreasing function of K : equivalently, if K is larger than its actual value, the fitted dodecanol concentration is larger than the nominal one.

5 Conclusion

Our experimental device allows us to explore the foam film rheological response in a large range of extension and extension rates. The film tension and extension are measured, and

we show that the film has a purely elastic behavior, that does not depend on the extension rate. The elastic modulus, defined in the linear regime, decreases with the SDS concentration and increases with the dodecanol concentration. At large deformation, we reach a non linear regime, which is rationalized with a model based on a local equilibrium of the film, and on a Langmuir coadsorption isotherm which parameters are taken in the literature. A good agreement is obtained between theory and experiment if a residual dodecanol concentration is assumed in the solution. The set-up provides a simple and efficient way to determine the local dynamical properties of the foam films.

Conflicts of interest

There are no conflicts to declare.

Acknowledgements

This project has received funding from the European Research Council (ERC) under the European Union's Horizon 2020 research and innovation programme (grant agreement No 725094).

Notes and references

- 1 J. W. Gibbs, *Transactions of the Connecticut Academy of Arts and Sciences*, 1876, **3**, pp. 108–248 and 343–524.
- 2 A. A. Sonin, A. Bonfillon and D. Langevin, *Phys. Rev. Lett.*, 1993, **71**, 2342.
- 3 G. Singh, G. Hirasaki and C. Miller, *J. Colloid Interface Sci.*, 1996, **184**, 92–105.
- 4 V. Bergeron, *Langmuir*, 1997, **13**, 3474–3482.
- 5 C. Stubenrauch and R. Miller, *J. Phys. Chem. B*, 2004, **108**, 6412–6421.
- 6 E. Santini, F. Ravera, M. Ferrari, C. Stubenrauch, A. Makievski and J. Krägel, *Colloids Surf., A*, 2007, **298**, 12–21.
- 7 D. Georgieva, A. Cagna and D. Langevin, *Soft Matter*, 2009, **5**, 2063–2071.
- 8 K. J. Mysels, M. C. Cox and J. D. Skewis, *J. Phys. Chem.*, 1961, **65**, 1107–1111.
- 9 A. Prins, C. Arcuri and M. van den Tempel, *J. Colloid Interface Sci.*, 1967, **24**, 84–90.
- 10 A. Prins and M. Van den Tempel, *J. Phys. Chem.*, 1969, **73**, 2828–2834.
- 11 H. Bianco and A. Marmur, *J. Colloid Interface Sci.*, 1993, **158**, 295–302.
- 12 V. Kovalchuk, A. Makievski, J. Krägel, P. Pandolfini, G. Loglio, L. Liggieri, F. Ravera and R. Miller, *Colloids Surf., A*, 2005, **261**, 115–121.
- 13 S. I. Karakashev, R. Tsekov, E. D. Manev and A. V. Nguyen, *Colloids Surf., A*, 2010, **369**, 136–140.
- 14 M. Durand and H. A. Stone, *Phys. Rev. Lett.*, 2006, **97**, 226101.
- 15 S. Besson and G. Debrégeas, *Eur. Phys. J. E: Soft Matter Biol. Phys.*, 2007, **24**, 109–117.
- 16 A. Bussonnière and I. Cantat, *J. Fluid Mech.*, 2021, **A25**, 1–52.
- 17 S. Cohen-Addad, R. Höhler and O. Pitois, *Annu. Rev. Fluid Mech.*, 2013, **45**, 241–267.
- 18 A. Bussonnière, E. Shabalina, X. Ah-Thon, M. Le Fur and I. Cantat, *Phys. Rev. Lett.*, 2020, **124**, 018001.
- 19 K. J. Mysels, K. Shinoda and S. Frankel, *Soap films: Study of their thinning and a bibliography*, Pergamon, New-York, 1959.
- 20 Y. Couder, J.-M. Chomaz and M. Rabaud, *Phys. D*, 1989, **37**, 384–405.
- 21 J. Lucassen and R. S. Hansen, *J. Colloid Interface Sci.*, 1966, **22**, 32–44.
- 22 C. Stenvot and D. Langevin, *Langmuir*, 1988, **4**, 1179–1183.
- 23 D. Vollhardt and G. Emrich, *Colloids Surf., A*, 2000, **161**, 173–182.
- 24 J. P. Fang and P. Joos, *Colloids Surf.*, 1992, **65**, 121–129.
- 25 M. van den Tempel, J. Lucassen and E. H. Lucassen-Reynders, *J. Phys. Chem.*, 1965, **69**, 1798–1804.
- 26 P. Joos and H. Deelstra, *Bull. Soc. Chim. Belg.*, 1975, **84**, 189–195.
- 27 D. Vollhardt and G. Czichocki, *Langmuir*, 1990, **6**, 317–322.
- 28 J. Lu, I. Purcell, E. Lee, E. Simister, R. Thomas, A. Rennie and J. Penfold, *J. Colloid Interface Sci.*, 1995, **174**, 441–455.